Antiprotonic Hydrogen

E. Klempt

Institut für Physik, Universität Mainz,
D-6500 Mainz, Fed. Rep. of Germany

Antiprotonic hydrogen is a positronium-like system, but its reduced mass is larger by a factor m_p/m_e and nuclear interactions play a significant role. Recent experiments at CERN have provided data which allow to test our understanding of the nuclear forces and of the atomic effects which govern the cascade of antiproton hydrogen from capture to annihilation.

1. Introduction

The discovery of antiprotons in 1955 by CHAMBERLAIN, SEGRE, WIEGAND, and YPSILANTIS /1/ was a great triumph for field theory and was honoured by the Nobel prize. Today antiproton beams of several 10^{11} antiprotons can be stored in the Antiproton Accumulator at CERN. The antiproton beam can be extracted and further accelerated. In collisions with protons at a center of mass energy of 540 GeV/c² particle jets are observed revealing the fundamental antiquark-quark scattering in Rutherford-like experiments; energetic electrons or muons manifest the existence of the gauge particles of weak interactions. On the other hand, the antiprotons can also be decelerated to 600 MeV/c and transferred to the Low Energy Antiproton Ring (LEAR). This ring, in operation since the end of 1983, allows to store 10^{10} antiprotons, to accelerate or decelerate antiprotons to all momenta between 70 MeV/c and 2000 MeV/c, to cool antiprotons in phase space, and to extract the particles into external beam lines. This operation results in intense ($>10^6$ $\bar{p}$/s) high-quality antiproton beams permitting experiments which were unfeasible before LEAR was built.

In the initial phase of the LEAR program there were three experiments (PS171, PS174 and PS175) searching for the characteristic lines of antiprotonic hydrogen atoms (protonium) /2-4/. Antiprotonic hydrogen atoms are formed by stopping antiprotons in H_2. The intensities of

The Hydrogen Atom Editors: G.F. Bassani · M. Inguscio · T.W. Hänsch

the lines were expected to depend strongly on target density. Since the optimum choice of the target density was not known, different densities were used in these experiments. The energies of the lines are dominantly given by the Coulomb interaction between proton and antiproton; the strong interaction leads to an additional energy shift and a line broadening. The measurement of these strong interaction effects was the primary motivation of these experiments. The strong density dependence of the line intensities indicates the presence of important atomic effects during the cascade which deserve interest on their own right.

Table I shows the basic properties of protonium, Fig. 1 the energy levels. Due to the change in reduced mass, the binding energy and

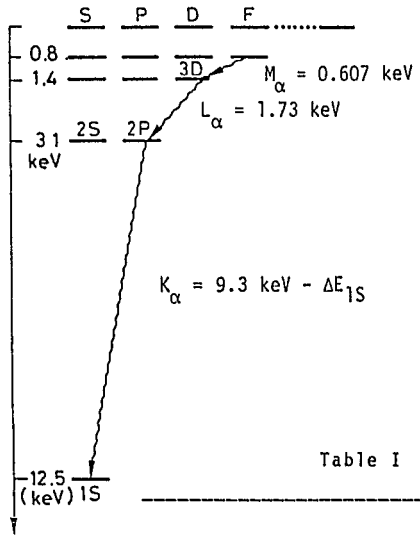

Fig. 1 Energy levels of protonium

Table I Basic Properties of Protonium

Reduced mass	$m_r = 1/2\ m_p$	=	469 MeV
Rydberg constant	$R = 1/4\ m_p c^2 \alpha^2$	=	12.5 keV
First Bohr radius	$a_0 = 4h/m_p c\alpha$	=	57 fm
Lyman series	$K_\alpha, K_\beta, .., K_\infty$	=	9.4, 11.1,..., 12.5 keV
Balmer series	$L_\alpha, L_\beta, .., L_\infty$	=	1.7, 2.4, .., 3.1 keV
Paschen series	$M_\alpha, M_\beta, .., M_\infty$	=	0.6, 1.0, .., 1.4 keV
Principle quantum number of Bohr orbit with $a_n(\bar{p}p) = a_0(H)$	n	=	30

transition energies are larger by nearly a factor of 1000 compared to ordinary hydrogen, the Bohr radii correspondingly smaller. The small size of the system allows the strong interaction to play a major role: the S and P wave atomic levels are shifted, and annihilation leads to a rather large width of these states. In states with higher angular momenta the strong interaction is too weak to lead to any observable consequences.

2. Identification of the Lyman Series

Fig. 2 shows the X-ray spectrum observed by PS171 in coincidence with antiprotons stopping in a H_2 gas target at NPT. The large peak at low energies is due to the unresolved Balmer series and some contamination from Argon fluorescence at 3 KeV. At higher energies a contribution from the Lyman series may be seen above a smooth background from Bremsstrahlung. The solid line represents the calculated Bremsstrahlungsspectrum (no fit). The data show the difficulties of protonium spectroscopy even using the excellent antiproton beams at LEAR: the yield of the Balmer series is 10% per antiproton stop, but a Balmer X-ray feeding one of the 2P levels is mostly not followed by radiative

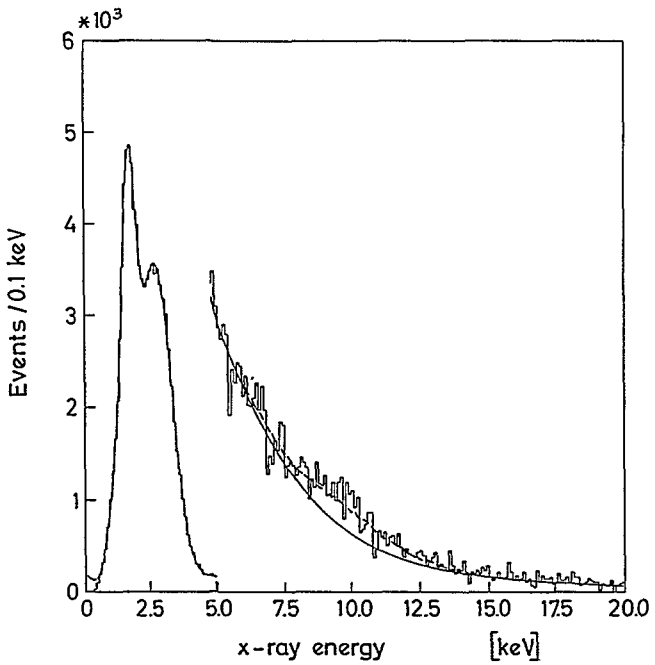

Fig. 2 X-ray energy spectrum of protonium in PS171. The solid line corresponds to the fit of the Balmer series and the calculated Bremsstrahlung. The dashed line represents possible Lyman contributions

emission of a Lyman-α line but by annihilation. The fraction of protonium atoms emitting a Lyman-α line is 1:1000; hence the experiments are forced to struggle against a high background produced in secondary reactions. In $\bar{p}p$ annihilation charged and neutral pions are produced, high energy γ-rays simulate low-energy X-rays by Compton scattering, negative pions lead to spectral lines of pionic atoms and to a neutron background by nuclear disintegration. In addition Bremsstrahlungs-quanta are emitted in the sudden acceleration of charged particles in the annihilation process.

The distinctive feature of PS171 is its capability to practically eliminate all these sources of background. This is achieved by a gaseous detector of very low mass. Compton scattering is correspondingly reduced, and solid material in which pions may stop is well separated from the target. The main source of background is the Bremsstrahlung. Energy and angular distributions of Bremsstrahlung can be calculated absolutely /5/, the agreement with the data is very good demonstrating the low background level which was achieved /6/. Bremsstrahlung can be avoided by triggering events in which protonium annihilate into neutral particles only. The residual background can then be eliminated by requiring that two X-rays should be observed in coincidence /7/.

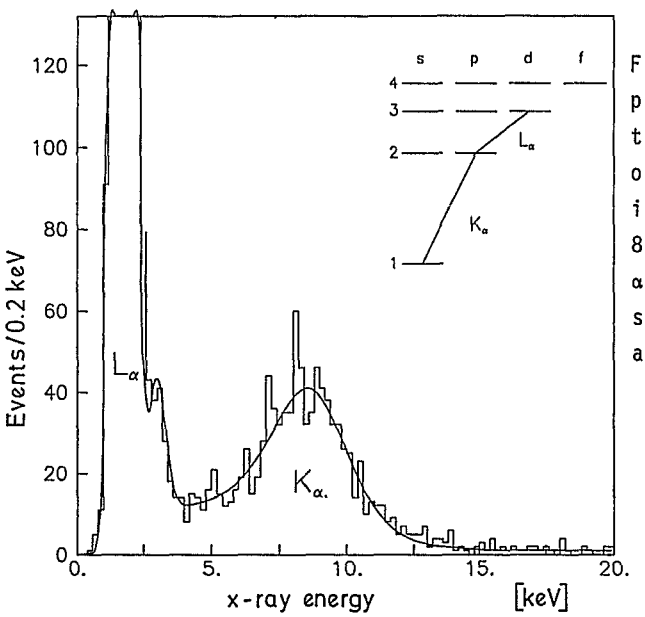

Fig. 3 X-ray spectrum of protonium. The energy of the more energetic X-ray of two coincident X-rays is shown. The peak at 8.5 keV is due to Lyman α lines (PS171). The line shape theory of ERICSON and HAMBRO /8/ is used

Fig. 3 shows the energy spectrum of X-rays for which a less energetic X-ray is observed in coincidence. The $\bar{p}p$ atom is required to annihilate into neutral particles only. This annihilation mode occurs with a rate of 4 %. The K_α peak is clearly seen. A number of checks confirm this interpretation: the distribution of X-ray energies observed in coincidence with the K_α peak shows the full Balmer series, the distribution of X-ray conversion points demonstrates that the X-rays originate out of the target, and gas analysis excluded the presence of contaminating lines. Hence the interpretation of the observed peak as K_α line with at most very few background events is unambiguous.

PS174 uses a conventional gas target of variable temperature in order to change the H_2 density. Extremely low pressures were achieved in experiment PS175. An inverse cyclotron was used to decelerate antiprotons to very low momenta, and antiprotons could be stopped with high efficiency at H_2 pressures as low as 30 mbar. Si(Li) solid state detectors (PS174, PS175) and gas scintillation proportional chambers (PS174) record the X-ray energy spectrum associated with antiprotons stopping in the target. Fig. 4 shows the data of PS174 recorded with two gas scintillation proportional chambers at 0.25 and 0.92 times the gas density at normal temperature and pressure /9/.

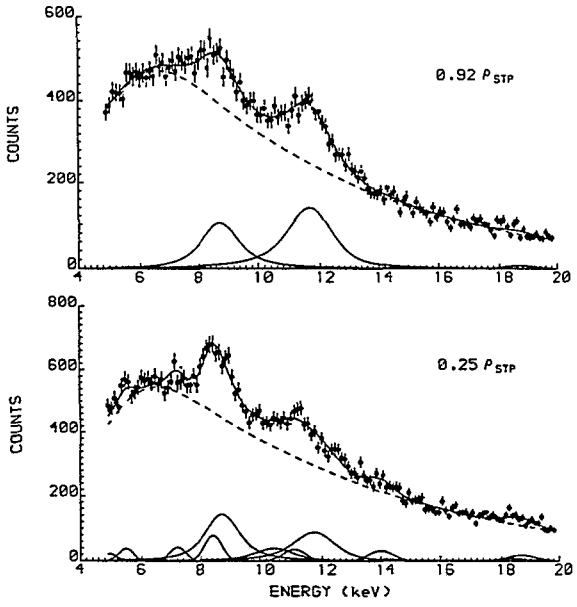

Fig. 4 X-ray spectrum of protonium (PS174). The solid line corresponds to the best fit taking into account the shape of the background from D_2 runs (dashed) and two Voigtian functions

H_2 and D_2 were used as target gases. Due to the higher absorption probability the yield of the Lyman series of $\bar{p}D_2$ is negligibly small, but the data can be used to identify the shape and the size of the background for the data taken with H_2. The data demonstrate clearly the existence of the K_α line.

The data sets gathered with Si(Li) detectors /10,11/ have a worse signal-to-background ratio but the results are consistent with the data shown above (see Fig. 6). Hence one can conclude that the same line is seen in different data sets.

3. Energy Shift and Width of the Ground State of Protonium

The line shape of the Lyman α radiation as observed in the detector is influenced by several effects:

1. The strong interaction leads to a finite width of the 1S state which is described by a Lorentzian line shape. The hyperfine splitting is estimated to be 200 eV. Therefore two lines with unknown fractional intensities are expected. Since the line width is much larger this splitting is not taken into account.

2. The electric dipole moment is not constant over the line. This effect requires a special lineshape theory which was developed by ERICSON and HAMBRO /8/. Not taking this effect into account leads to an apparent shift of the peak to higher energy.

3. The detection efficiency over the line spectrum is not constant as a function of energy. For gaseous targets it falls with increasing energy resulting in an apparent shift of the observed peak to lower energies.

4. The finite detector resolution leads to an additional broadening of the line.

Neglecting point 2 and 3 leads to the well known Voigt function which is used by PS174 and PS175. However, PS171 finds a large dependence of the fit results on line shape theory and on the energy dependence of the detection efficiency; therefore the data of PS171 are fitted with a convolution of all four effects. The final results

Table II ΔE_{1S}, Γ_{1S}, and Γ_{2P} of protonium

Experiment	Energy shift ΔE_{1S}(keV)	Width Γ_{1S}(keV)	Width Γ_{2P}(MeV)
PS171	-0.70(15)	1.60(40)	
PS174 a	-0.73(5)	1.13(9)	
PS174 b	-0.75(6)	0.90(18)	45(10)
PS175	-0.66(13)	1.13(23)	40(11)
Theory			
Richard and Sainio	-0.73	0.94	26
Moussallam	-0.75	1.00	27

of all three experiments are presented in Table II and compared to two recent theoretical results /12,13/. The agreement between experiment and theory and in between the different theoretical models is rather good.

Very likely the essential ingredients for an understanding of the strong interaction effects are the Coulomb potential, π exchange and annihilation. The annihilation suppresses the central part of the protonium wave function with a large contribution to the binding energy. This leads to less binding even though the nuclear interaction is basically attractive. The theoretical models use the same π exchange potential amd phenomenological annihilation potentials fitting low-energy cross-sections; since short range interactions (in which different One-Boson-Exchange models differ) are suppressed by annihilation, all models give very similar results.

4. The 2P Strong Interaction Width

The data of Fig. 2 demonstrate that the 2P level has a strong interaction width Γ_{2P} exceeding the radiative width Γ_{rad} by about two orders of magnitude. These data can, however, not be used to determine Γ_{2P} since the fraction of neutral annihilation of the hyperfine levels of the 2P and 1S levels is not known. An average Γ_{2P} can be obtained by not triggering on specific annihilation modes. Fig. 5 shows the Balmer series, Fig. 6 the Lyman series of PS174 taken with a solid state Si(Li) detector at two different H_2 gas densities. The

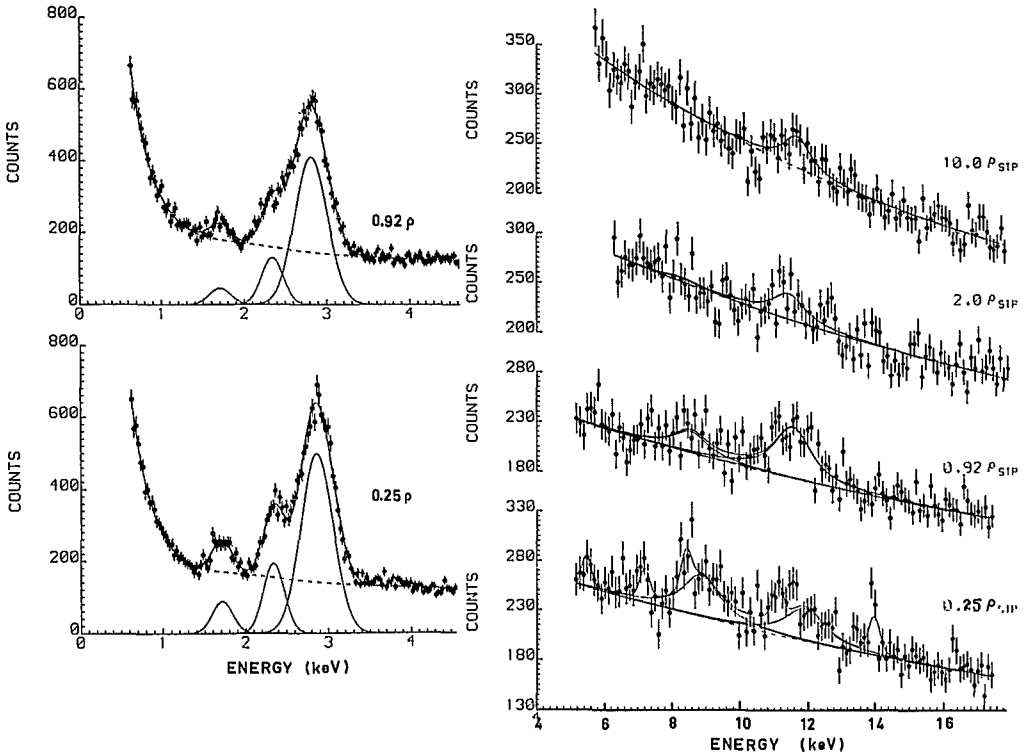

Fig. 5 and 6 X-rays from protonium (PS174), Si(Li) detector. Balmer series (left) and evidence for the Lyman series are shown as a funtion of H_2 gas density

detection efficiency at these low energies is a steeply rising function; it was calculated by Monte Carlo techniques. From this the strong interaction width of the 2P levels weighted with the (unknown) fractional populations of the 2P levels were determined. The result is also shown in Table II. The large strong interaction width of the 2P levels is provoked by the tunnel effect: the protonium wave function may tunnel through the centrifugal barrier into the region of strong interaction in which annihilation is extremely strong. This simple picture is capable of a quantitative description of Γ_{2P}.

5. Cascade

Fig. 6 shows that the X-ray intensities depend strongly on the density of the H_2 target. When antiprotons are stopped in H_2 they are captured into high Rydberg states of protonium: the H_2 molecule dissociates and the electron of one H atom is ejected by Auger emission. The subsequent cascade results from a competition of density dependent and density independent effects: in collisions $\bar{p}p$ atoms experience high electric field strengths of 10^{12} V/m leading to a reshuffling of states with different angular momenta; the Coulomb interaction between $\bar{p}$ and atomic electrons may lead to external Auger effect resulting in a de-excitation of the $\bar{p}p$ atom; radiative transition may occur, and annihilation from protonium states with angular momenta 0 or 1 may stop the atomic cascade. Recently, we have calculated these processes /14/. Results of the calculations are shown in Fig. 7. The

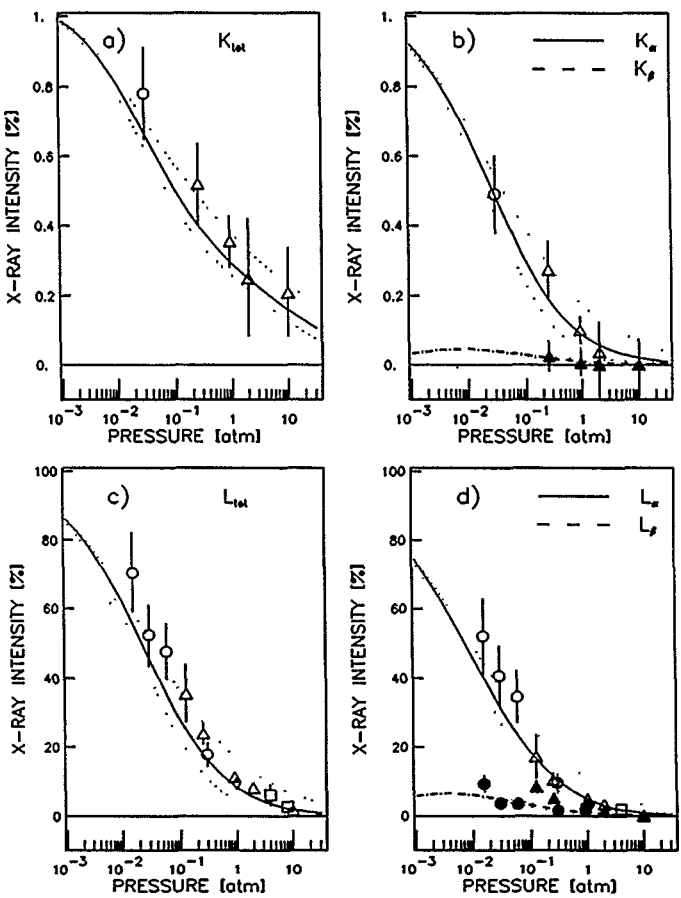

Fig. 7 Cascade of protonium in H_2 gas. The data are from PS171, 174 and PS175. The solid line represents an absolute calculation, the dotted lines two extreme variations of the calculated Auger effect

good agreement between the experimental result and the calculation - which uses no fit parameter - demonstrates the good understanding of the atomic physics in antiprotonic hydrogen atoms.

References

/1/ O. Chamberlain, E. Segrē, C. Wiegand, Th. Ypsilantis: Phys.Rev. 100, 947 (1955)
/2/ R. Armenteros et al.: A study of $\bar{p}p$ interactions at rest in a H_2 gas target at LEAR. CERN, PS171 (1980). In Experiments at CERN, Geneva (1987)
/3/ E.W.A. Lingman et al.: Precision Survey of X-rays from $\bar{p}p$ ($\bar{p}d$) Atoms. CERN PS174 (1980) ibid.
/4/ R. Bacher et al.: Measurement of the Antiprotonic Lyman- and Balmer X-rays of $\bar{p}H$ and $\bar{p}D$ Atoms. CERN, PS175 (1980)
/5/ R. Rückl and C. Zupancic: Phys.Lett. B150, 225 (1985)
/6/ U. Schäfer et al.: "X-rays from proton antiproton annihilation into charged final states", submitted to Phys.Lett. B
/7/ M. Ziegler et al.: Phys.Lett. B206, 151 (1988)
/8/ T.E.O. Ericson and L. Hambro: Annals of Physics 107, 44 (1977)
/9/ C.W.E. van Eijk et al.: Nucl.Phys.A (in print)
/10/ C.A. Baker et al.: Nucl.Phys. A483, 429 (1988)
/11/ L. Simons: "Results from antiprotonic atoms at LEAR", in Physics at LEAR with low energy antiprotons, eds. C. Amsler et al., (Harwood Academic Publishers, Chur 1988), p. 703
/12/ J.M. Richard and M.E. Sainio: Phys.Lett. B110, 349 (1982)
/13/ B. Moussallam: Z.Physik A325, 1 (1986)
/14/ G. Reifenröther and E. Klempt: Antiprotonic Hydrogen: From Capture to Annihilation, MZ-ETAP/88-11